



RETRACTED: Dispersed Ag₂O/Ag on CNT-Graphene Composite: An Implication for Magnificent Photoreduction and Energy Storage Applications

Mohamed Mokhtar Mohamed 1, M. Khairy 1,2* and Ahmed Ibrahem

¹ Chemistry Department, Faculty of Science, Benha University, Benha, Egypt, ² Chemistry Department, College of Science, Al-Imam Mohammad Ibn Saud Islamic University, Riyadh, Saudi Arabia, ³ Duravit, Heliopolis, Egypt

OPEN ACCESS

Edited by:

Sotiris Sotiropoulos, Aristotle University of Thessaloniki, Greece

Reviewed by:

Siddharth Surajbhan Gautam, The Ohio State University, United States Sugata Chowdhury, National Institute of Standards and Technology, United States

*Correspondence:

M. Khairy mohkhairy@fsc.bu.edu.eg

Specialty section:

This article was submitted to Physical Chemistry and Chemical

> a section of the journal Frontiers in Chemistry

Received: 29 March 2018 Accepted: 08 June 2018 Published: 03 July 2018 Retracted: 29 October 2025

Citation:

Mohamed MM, Khairy M and Ibrahem A (2018) Dispersed Ag₂O/Ag on CNT-Graphene Composite: An Implication for Magnificent Photoreduction and Energy Storage Applications. Front. Chem. 6:250. doi: 10.3389/fchem.2018.00250

A simple hydrothermal route assisted by a triblock copolymer was used to synthesize Ag₂O/Ag nanoparticles on a robotic support consists of functionalized MWCNTs and graphene composite (Ag₂O/Ag/CNT-graphene). The composites together with the individual analog of Ag/CNT and Ag/graphen were characterized by means of XRD, TEM-SAED, N₂ sorptiometry, Raman, FTIR, UV-Vis, and photoluminescence spectroscopy. These nanomaterials were then tested for the catalytic reduction of 4-nitrophenol (4-NP) to the technologically beneficial 4-aminophenol (4-AP). The Ag₂O@Ag@CMT-graphene composite calcined at 400°C has shown fascinating reduction performances for 4-NP either in the dark $(k = 0.014 \text{ s}^{-1})$ or under visible light illumination $(k = 0.039 \text{ s}^{-1})$ in the presence of 5 mM NaBH₄ compared to Ag/CNT (0.0112 s⁻¹) and Ag/graphene (0.010 s⁻¹) catalysts. This was chiefly because Ag₂O@Ag@CNT-graphene comprises the highest pore volume (0.49 cm³/g) and involves three types of pores in the margin from 1.8 to 4.0 nm in front of only one modal type f pores for the rest of the catalysts and thus maximizes the adsorptive capacity of the reactants (4-NP and NaBH₄). Moreover, the former composite exhibits the highest concentration of the Ag₂O component as established by numerous techniques in addition to the cyclic voltammetry, proposing it's facile reaction with 4-NP along with the simultaneous transfer of surface hydrogen and electrons from NaBH4 ions to produce 4-AP. The promotion of the p-n junction evaluated using the Mott-schottky equation on Ag₂O@Ag@CNT-graphene assisted by charges separation and surface plasmon resonance bands of Ag and Ag₂O are found to be advantageous for 4-NP reduction. The latter composite delivers a specific capacitance of 355 F g⁻¹ at 1.0 A g⁻¹ exceeding those of Ag/CNT (230 F g⁻¹) and Ag/graphene (185 F g⁻¹). The EIS study establishes the high electronic conductivity of the metallic Ag and Ag₂O moieties, low internal resistance of CNT-graphene as well as the marked ionic transfer facilitated by the composite porous nature.

Keywords: Ag₂O@Ag/CNT-graphene, 4-nitrophenol reduction, p-n junction, various additives, supercapacitor

1

INTRODUCTION

Oxygen-containing CNTs are desirable rather than pristine CNTs since the former are considered as anchoring sites for diverse semiconductors and metal nanoparticles via forming covalent, electrostatic and hydrogen bonds (Broza et al., 2005; Wang et al., 2010). Controlling the extent of oxidation as well as its conditions is a prerequisite to avoid corrosion and CNTs structure disturbance. On the other hand, such oxides affect negatively the conductivity of CNTs as well as its thermal stability (Hu et al., 2004; Guo et al., 2010), which restrict their use in lots of applications. In order to avoid the loss of conductivity of functionalized CNT, a hybridization with graphene nanosheet was manufactured to produce a highly conductive nanocomposite. Such composite has attracted much attention in various applications most importantly in high electronic conductivity, mechanical energy, optoelectronics and sensors (Geim and Novoselov, 2007; Geim, 2009; Sun et al., 2013). More applications in catalysis still remain to be discovered based on the promising intrinsic properties of functionalized CNTs and when inter-dispersed with graphene nanosheets. The challenge here is to prepare a highly dispersed graphene-CNT structures with controlled interlayer functional groups and maintain the metal (oxide) incorporation as well as their combined conductivity. Other important characteristics including wettability, adsorption and electrophilicity are also affected by the way of modification performed during the synthesis of the CNT-graphene hybrid materials, which by its turn will influence their catalytic applications (Eda and Chhowalla, 2010; Liu et al., 2015). The CNT-graphene composite modified with the metal nanoparticles provides a new model for boosting the reduction efficiency based on the synergistic interaction between CNT and graphen aided by the grown Ag₂O and Ag moieties. Undeniably, silver nanoparticles have attracted lots of attention in different areas of application; however, the agglomeration and the consequent separation processes prohibit its usage. This can be minimized by affixing the Ag nanoparticles on CNTgraphene composite. Indeed, the functionalized CNT is going to show a p-type transfer that can be converted after graphene incorporation and with the deposited Ag into ntype compensated by the p-type Ag₂O formed species. The formation of the p-n junction between oxygen functionalized CNT/Ag₂O (as p-type) and Ag/graphene (as n-type) heterostructure [CNT/Ag₂O/Ag/graphene] is expected to enhance the reduction activity based on enhancing the conductivity, electron mobility and lifetime of photo-generated electronhole pairs. This work inspects the relationships between the photocatalytic activity and structure alterations in view of metal (oxide)-support interaction, average metal size and dispersion, charge transfer, role of surface texturing, and functionalities of Ag₂O/Ag/CNT-G on the reduction efficiency of nitrophenols. The supercapacitance performances of the catalysts is estimated and well correlated with the photocatalysts structure as well as their photo-reduction effectiveness.

EXPERIMENTAL

Catalysts Preparation

0.5 g of the as-obtained multi-walled carbon nanotubes (of length equal 10-30 μ m, purity >95%, S_{BET} >500 m²/g and EC of 10² S/cm) and 0.5 g of the as-fabricated graphene oxide (according to the modified Hummer method) are dissolved in 10 ml of the synperonic F108 (Triblock copolymer of an average M_n 2800-Sigma Aldrich), formed as a result of dispersing 1 g/100 ml distilled water. To the latter suspension, an aqueous AgNO3 solution (to from 4 wt%Ag) dissolved in 10 ml distilled water was well mixed and kept under stirring for 30 min followed by sonication for another 3.0 h. During the latter sonication process, an addition of NaBH4 (0.1 M) is began till the yellow color is formed. Later on, this suspension is autoclaved at 180°C for 12 h followed by washing, filtering and drying at 100°C for 5 h. This catalyst was finally annealed at 400°C, and to be denoted as 4%Ag/CNT-graphene₄₀₀. Similarly, the individual analog 4%Ag/CNT₄₀₀ and 4%Ag/graphene₄₀₀ catalysts are prepared in a typical way to that mentioned for the hybrid CNTgraphene.

Characterization Techniques

X-ray diffraction (XRD) was measured at room temperature using a Philips diffractometer (Model PW-3710). The patterns were progressed with Ni-filtered copper radiation ($\lambda = 1.5418$ Å) at 30 kV and 10 mA with a scanning speed of $2\theta =$ 50/min. The Fourier transform infrared (FT-IR) spectra were monitored via a single beam using Thermo scientific Nicolet iS10 instrument thorough which the samples were grounded with (Br (1:100) to form tablets, and to record the measurements in the 4,000-400 cm⁻¹ region. The surface texturing properties namely BET surface area, total pore volume (Vp) and mean pore radius (r) were determined from N2 adsorption isotherms measured at 77 K after out-gassing the samples at 473 K for 3 h under a reduced pressure of 10^{-5} Torr. Diffuse reflectance ultraviolet-visible spectroscopy (UV-vis DRS) of the samples was carried out at room temperature using UV-vis JASCO spectrophotometer (V-570) in the of 200-1,000 nm range using BaSO₄ as a standard. The band gap energy (Eg) of the samples is estimated using the equation: $\alpha h \nu = A(h \nu - E_g)^{n/2}$ and determined by finding the intercept of the straight line of the plot of $(\alpha h \nu)^{1/2}$ or $(\alpha h \nu)^2$ against hv for both indirect and direct transitions, respectively (Ibrahim et al., 2016). TEM micrographs were measured using a JEM-2100 model which achieves high resolution of 0.19 nm at a power of 100 kV. Selected area electron diffraction (SAED) images were also recorded at an accelerating voltage of 100 kV. The photoluminescence (PL) excitation and emission spectra were measured on a thermo scientific fluorescence spectrophotometer model Lumina. The measurements were conducted at room temperature using a He/Cd laser (310 nm) as an excitation source. Raman spectra were measured with a U-1000 laser Raman spectrometer using the 514.5 nm line of an ArC laser as the excitation beam. Electrochemical measurements including cyclic voltammetry (CV) were determined using Digi-Ivy 2116 B, USA, in 6.0 M

KOH aqueous solution as well as the electrochemical impedance spectroscopy (EIS) was determined using Metrohm autolab PGSTAT204; equipped with Nova 1.11 software for data calculation and fitting. More details information about the measurement conditions can be found elsewhere (Mohamed et al., 2017).

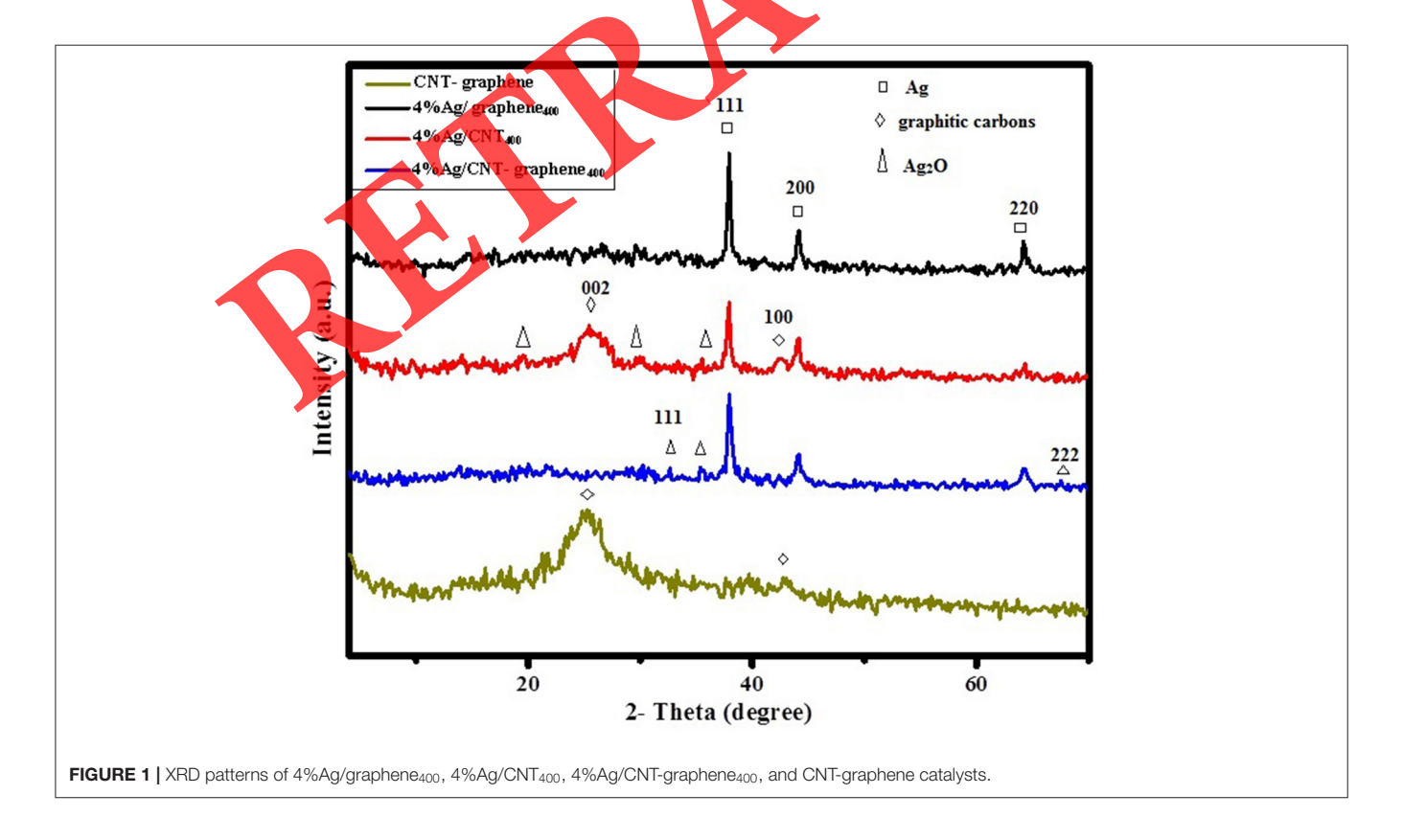
Catalytic Reaction

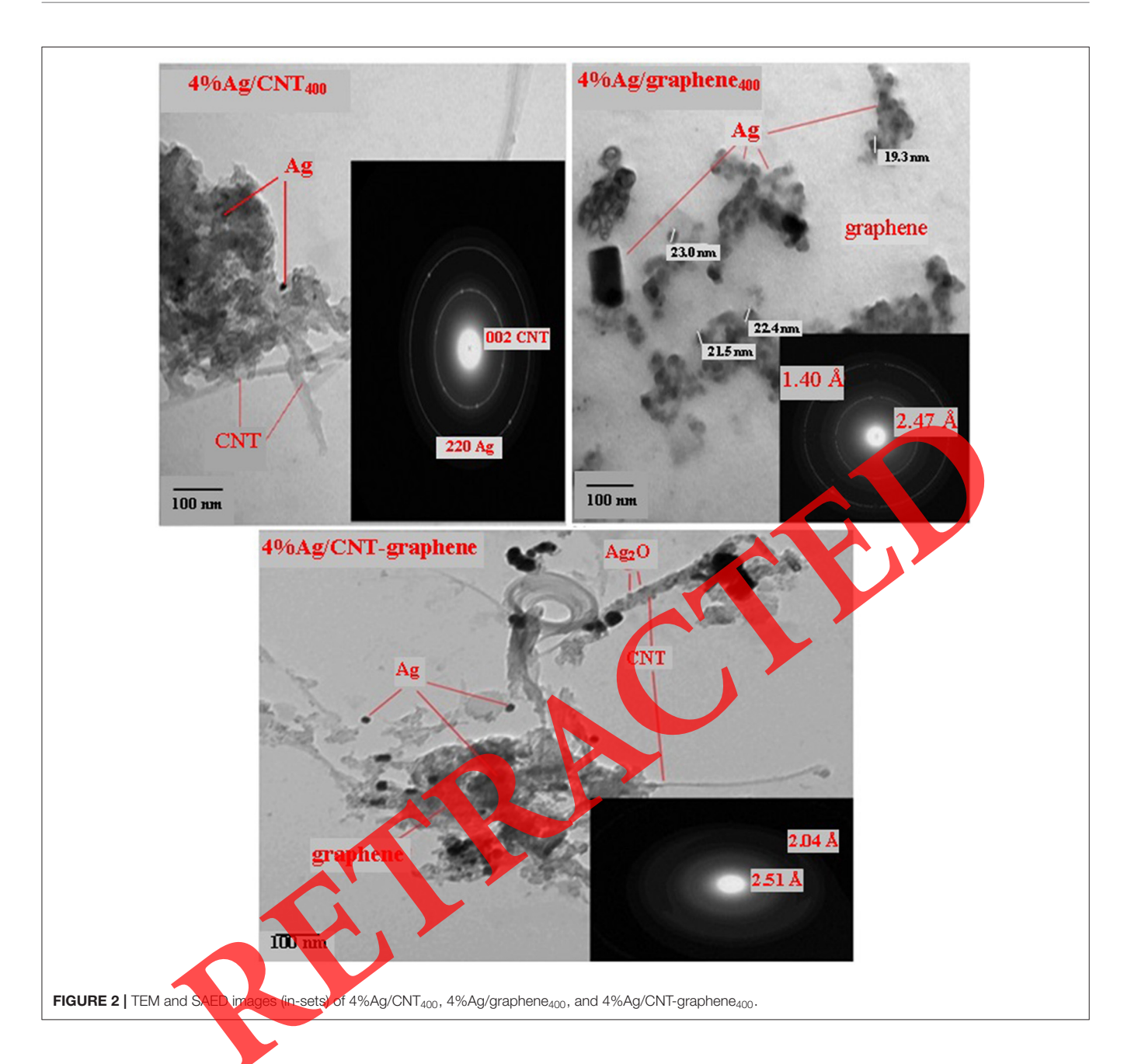
To investigate the catalytic reduction of 4-nitrophenols (4-NP), 100 ml of 0.1 mmol aqueous solution of 4-NP was inserted in a 100 ml beaker together with a 12.5 ml of 0.5 M of NaBH₄. The solution was subjected to a constant stirring. With the addition of NaBH4, the yellow color of the solution was darkened due to the formation of the phenolate ions. The desired amount of catalysts was added (0.025 g); while stirring was continued at room temperature. The dark yellow color of the solution was progressively vanished, demonstrating the reduction of 4-NP. The reaction progress was checked via withdrawing samples from the reaction mixture at normal time intervals. The catalyst/4-NP+NaBH₄ suspension was also exposed to the visible light irradiation of a 160 W Hg lamp, to investigate the effect of light on the reduction activity of the catalyst. The conversion of 4-NP to the corresponding amino (4-AP) was checked by UV-Visible spectroscopy (a Perkin Elmer Lamda-900) by measuring the absorption maxima corresponding to the reactant 4-NP as well as the product 4-AP compounds. For the recycling measurement, the used catalyst was separated by filtration and then used without any treatment for further six times under the same conditions. The effect of additives on the catalysts performances toward 4-NP reduction was performed by adding 100 ppm concentration of triethanol amine, isopropyl alcohol, benzoquinone and Na₂CO₃.

RESULTS AND DISCUSSION

Catalysts Characterization

The X-ray diffraction profiles of Ag incorporated graphene, CNT and CNT-graphene catalysts calcined at 400°C were shown in Figure 1. The peaks correspond to Ag nanoparticles having fcc crystal structure (JCPDS no. 04-0783) were found in all samples via exposing the crystal planes of (111), (200), and (220). The Ag nanoparticles diffraction peaks were more intense on the graphene sample proposing higher crystallites size and lower dispersion. Additionally, the Ag₂O phase (JCPDS card no. 41-1104) exhibited via the main diffraction plane (111) at 32.8°; beside some others at $2\theta =$ 36.2° and 19.7°, shows an enhancement mostly on the 4% Ag/CNT-graphene₄₀₀ catalyst. Graphitic peaks due to (002) and (100) planes were only shown on the CNT sample; when compared with the mother CNT-graphene pattern, indicating that the deposition of Ag NP can prevent the stacking of graphene when interconnected with CNT into multilayers (Thao et al., 2013). More information concerning the structure and distribution of Ag/Ag₂O nanoparticles on the different substrates were provided by TEM-SAED characterization shown in Figure 2. The TEM image as vell as the SAED pattern of 4%Ag/CNT400 indicates the



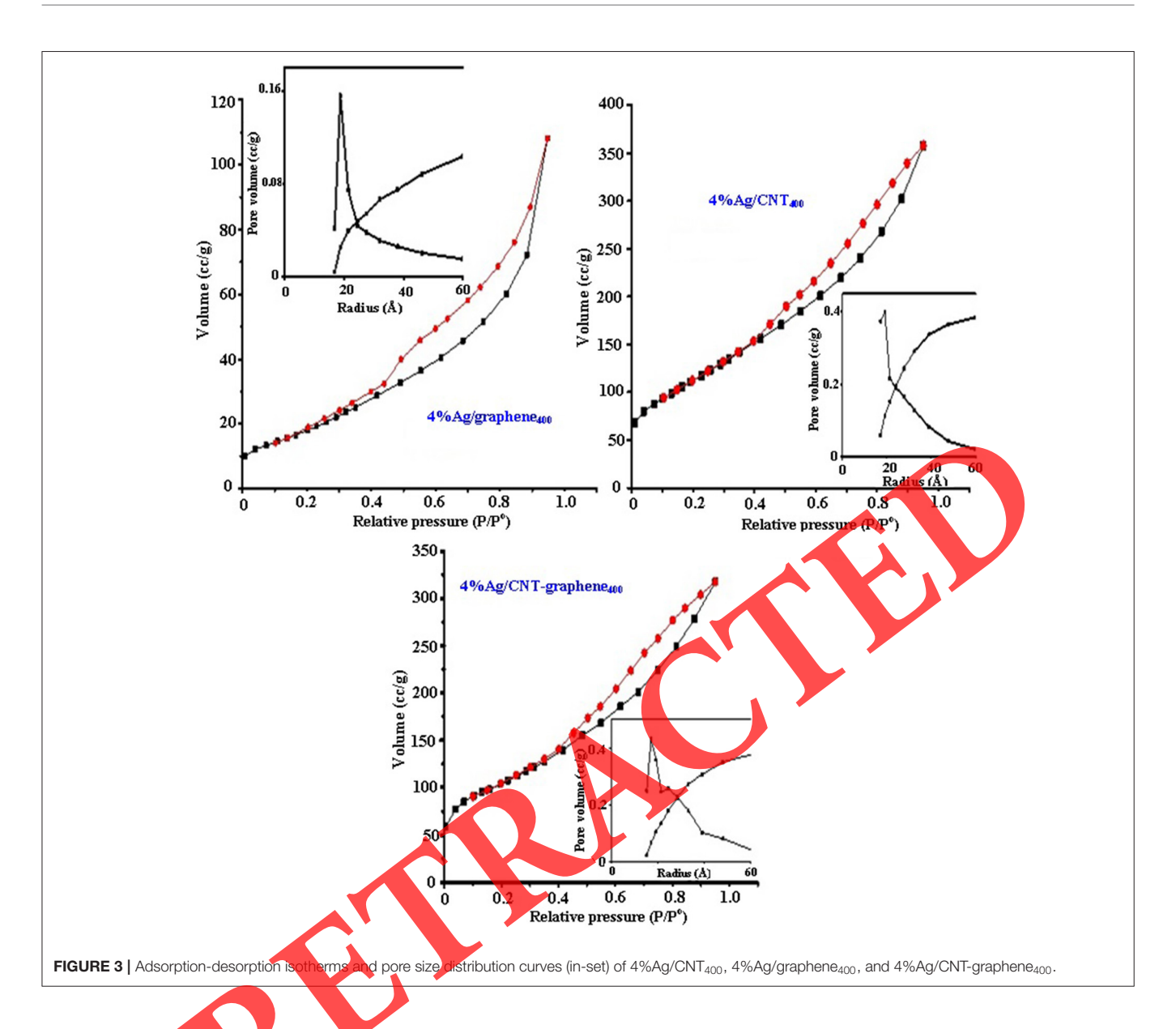


existence of homogenously dispersed Ag nanoparticles on CNTs; evidenced by the existed lattice plane (220), with an average diameter of 7 nm. The HRTEM shows a little deterioration for the CNTs networks as a result of the high calcination temperature. The TEM image of 4%Ag/graphene₄₀₀ exhibits an agglomeration of Ag nanoparticles of a dimension with 23 nm. The SAED inset-image evidences the presence of lattice fringes with interplanar spacing of 2.47 and 1.40 Å due to (002) and (220) diffraction planes of graphene and Ag nanoparticles, respectively, supporting the results obtained from XRD investigation. The TEM image of the 4%Ag/CNT-graphene₄₀₀ catalyst shows that graphene coated carbon nanotube and silver nanoparticles of spherical architecture are equally distributed on both of the

TABLE 1 | Surface texturing properties of the synthesized catalysts.

Samples	Surface texturing		
	S _{BET} (m ² /g)	Pore radius r- (Å)	Pore volume Vp ^{total} (cm ³ /g)
Ag/graphene ₄₀₀	71	46.9	0.167
Ag/CNT ₄₀₀	413	22.4	0.461
Ag/CNT-graphene ₄₀₀	365	26.8	0.490

carbon substrates. The distributed Ag nanoparticles of darker color and of average diameters of 20 nm were seen throughout the image. A lighter color is seen mainly around CNTs to ascribe

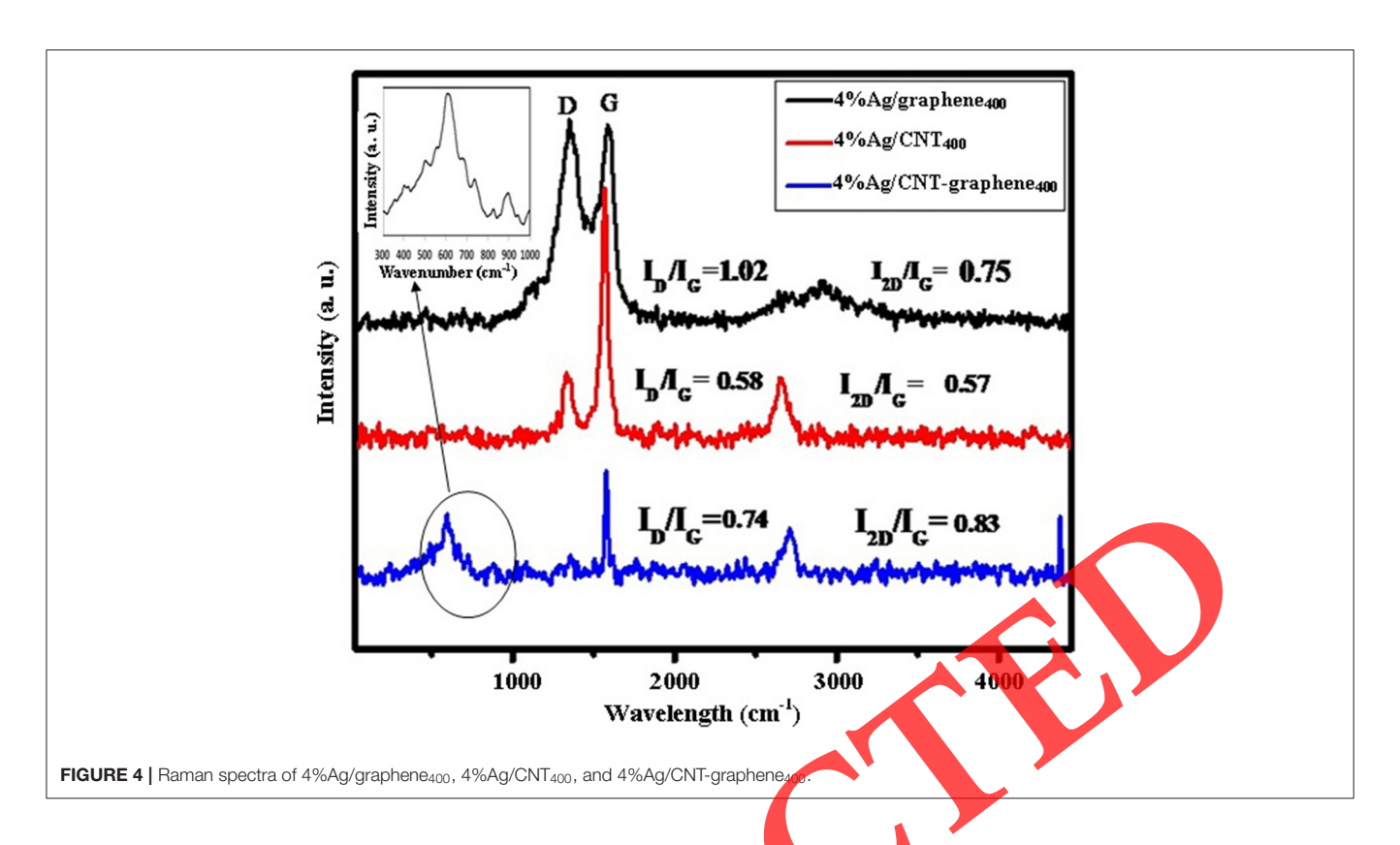


the presence of the Ag₂O phase; in agreement with XRD results, of a mean diameter of 15 nm. The SAED pattern of this sample demonstrates diffraction bright spots at d-spacings 2.51 and 2.04 Å corresponding respectively, to the (002) and (200) planes of graphitic carbons and Ag nanoparticles, respectively.

Nitrogen sorptiometry experiments revealed that the pore diameter was the widest in the Ag/graphene₄₀₀ sample (46.8 Å) and thus showed the lowest S_{BET} value (71.4 m²/g) if compared with Ag/CNT₄₀₀ (412.7 m²/g) and Ag/CNT-graphene₄₀₀ (365.1 m²/g), depicted in **Table 1**. The latter sample shows the deepest pore volume value (0.490 cm³/g) with a median pore size of 26.9 Å. All the prepared materials exhibited a characteristic Type IV isotherm (**Figure 3**), with a hysteresis closure at p/p° of 0.4 where it shifted into 0.2 for Ag/graphene₄₀₀, revealing the presence of some narrower pores. The pore size distribution graphs (insets in **Figure 3**) indicates a mono-modal type of pore at 20 Å for Ag/CNT₄₀₀ and Ag/graphene₄₀₀ samples whereas for

Ag/CNT-graphene $_{400}$ three modal type of pores at 18, 20, and 40 Å are depicted. This indeed reflects the strong hybridization occurred between CNT and graphene structures.

The Raman spectra of Ag incorporated graphitic carbons exhibit two peaks at 1,354 and 1,590 cm⁻¹ due to the D-and G bands, respectively (**Figure 4**). The ID/IG ratio was found to be the least in 4%Ag/CNT₄₀₀ (0.58) compared to 4%Ag/CNT-graphene₄₀₀ (0.74) whereas 4%Ag/graphene₄₀₀ retains the ratio of 1.02 similar to that without Ag, pertaining higher graphitization purity and least disturbance. This indeed maximizes the occurred defects in former catalysts comparatively and to comprehend the strong interaction of the Ag nanoparticles within their structures. The 4%Ag/graphene₄₀₀ sample shows a more diffused and splitted 2D band (2,800–3,000 cm⁻¹) with higher wavenumber than those exhibited on the former ones (2,730–2,750 cm⁻¹), proposing an extra contribution of the inner double-resonance scattering due to layers of graphene sheets. The



appearance of a Raman peak at 594 cm⁻¹ solely on 4%Ag/CNT-graphene₄₀₀ confirms the existence of Ag-O stretching modes (Sheng et al., 2012).

The FT-IR spectrum (400–4,000 cm⁻¹) of the fabricated CNTgraphene, shown as inset in Figure 5, indicates peaks correlated to the O-H stretching of the hydroxyl group at 3,408 beside peaks at 2,919 and 2,850 cm⁻¹ due to asymmetric and symmetric stretching of the C-H bond, in CH₂, and 1,565 cm⁻¹ with 1,451 cm⁻¹ to the aromatic C=C stretching, confirming the hexagonal structure of the graphitic carbons and indeed indicative of the intact structure of CNT and graphene without disruption following the hybridization process (Armani et al., 2016). The peaks in the margin between 1,388 and 1,046 cm⁻¹ correlated to C-OH and C-O stretching vibrations together with peaks at 1,711 cm⁻¹; associated with the C=O, and at 711 cm⁻¹; due to the O-H bending vibration, were also revealed. A reduction in the 3,414 cm $^{-1}$ peak is noticed in the 4%Ag/CNT₄₀₀ spectrum. This latter spectrum also retained back all the peaks correlated to C-O-C and C-OH stretching beside the carbon double bond (C=C) vibration but with a significant decrease in intensity. This catalyst also provokes the evolution of Ag-O moieties as diagnosed via the peak at 560 cm⁻¹. In case of 4%Ag/graphene₄₀₀, vanishing of the free OH band is attained together with reducing the intensity of all the bands correlated to C=O, C-O, C-OH, and C-O-C functional groups, those suffer blue shifting compared to the Ag free sample to simply comprehend the Ag involvement. The presence of bands at 943, 825, 700, and 615 cm⁻¹ never seen in the hybrid spectrum can be correlated to the involvement of Ag and Ag-O bonds within graphene structure (Carboni et al., 2014). Similarly, the free OH group was dimmished in the 4%Ag/CNT-graphene₄₀₀ spectrum and instead hydrogen bonded one at 3,073 cm⁻¹ was delivered. The revealed bands at 950 and 486 cm⁻¹ those never seen in CNT-graphene are indicative to the presence of Ag₂O vibrations (Carboni et al., 2014).

Figure 6A shows UV-Vis DRS of Ag loaded different graphitic catalysts for evaluation of their absorption capabilities. Three different types of peaks were seen for the three catalysts within the margin 260-280, 290-300, and 310-360 nm. They sequentially attributed to π - π *, n- π * and to the highly dispersed Ag in CNT and CNT-graphene catalysts. The 4%Ag/graphene₄₀₀ catalyst showed a higher visible light sensitivity than rest or the catalysts beside a surface plasmon resonance band at 525 nm. Whereas, 4%Ag/CNT₄₀₀ and 4%Ag/CNT-graphene₄₀₀ catalysts showed an SPR band around 460 nm. This blue shift could arise from the charge transfer to the nanoparticle domain surface. Tauc band gap calculated values between $(\alpha h \nu)^2$ and $(h \nu)$ (**Figure 6B**) were 1.55, 2.6, and 2.5 eV for 4%Ag/graphene₄₀₀, 4.0%Ag/CNT₄₀₀, and 4%Ag/CNT-graphene₄₀₀, respectively. To have a clue about photoelectron transition via different composites and to check their photo-carriers recombination, the photoluminescence (PL) spectra were measured following an excitation at 320 nm (Figure 7). All the samples indicate strong emissions at 420 (2.9 eV), 470 (2.64 eV), and 530 nm (2.34 eV) and specifically the first peak shifted into 425 nm in 4%Ag/CNT-graphene₄₀₀ proposing stronger interaction of the Ag with the hybrid structure composed of CNT-graphene. The wide SPR absorption seen at 530 nm probably signifies the presence of the band gap

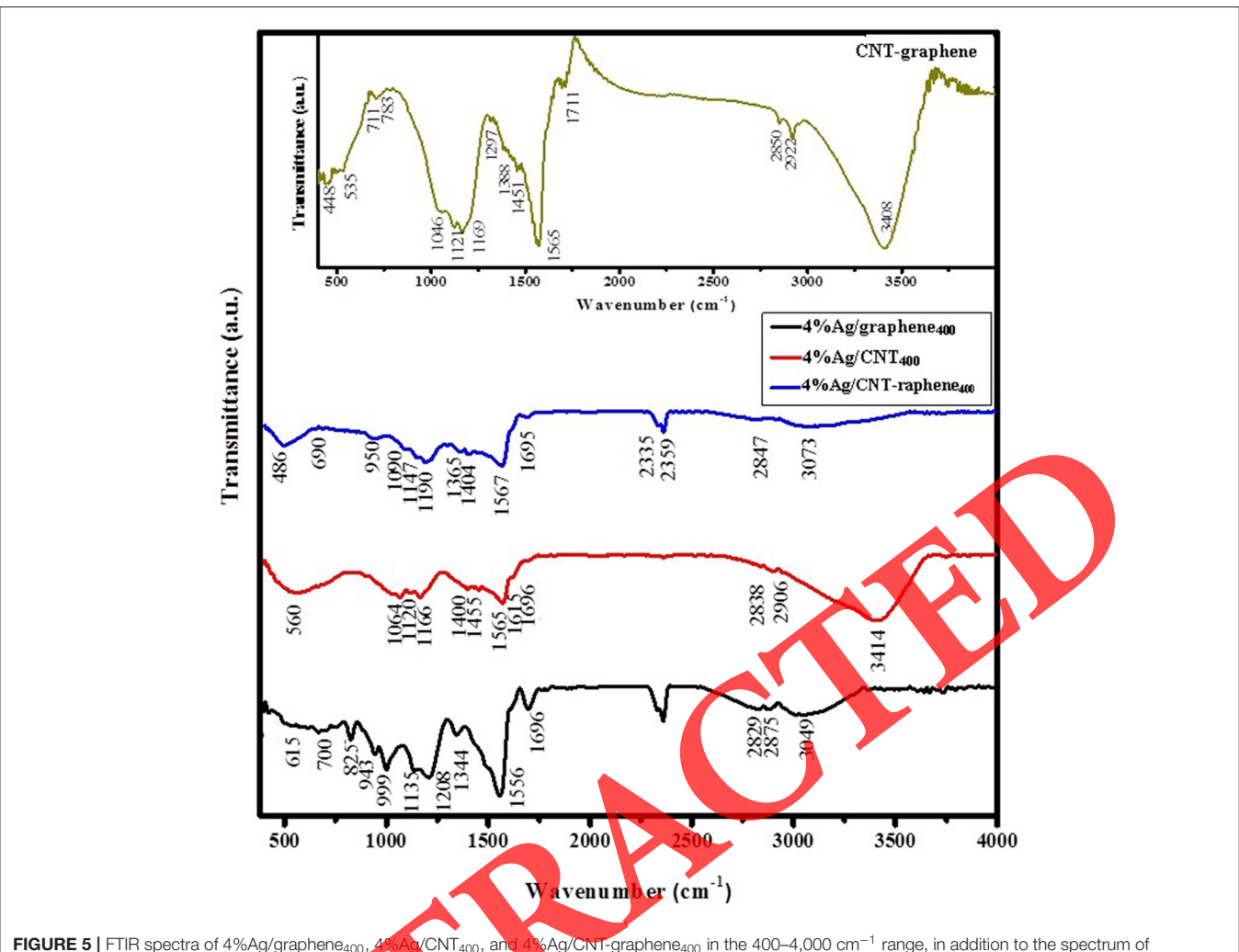


FIGURE 5 | FTIR spectra of 4%Ag/graphene₄₀₀, 4%Ag/CNT₄₀₀, and 4%Ag/CNT-graphene₄₀₀ in the 400–4,000 cm⁻¹ range, in addition to the spectrum of CNT-graphene as in-set.

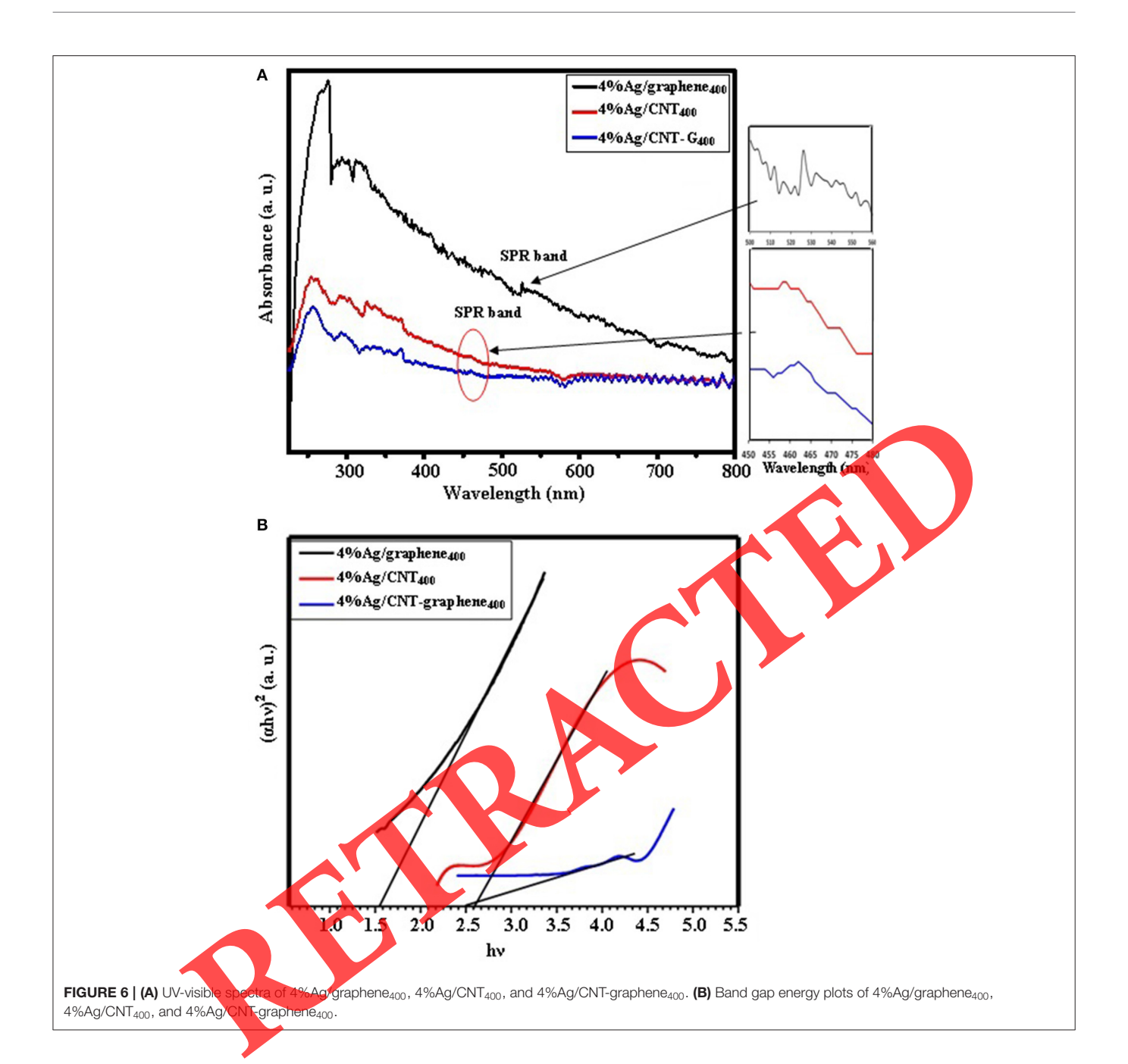
transition of the Ag₂O NPs (Pan et al. 2012). This was in harmony with the UV-Vis diffuse reflectance results. A significant decrease in the enrission intensity of 4%Ag/CNT-graphene₄₀₀ compared to the rest of the samples was shown due to weak light-matter interaction, suggest lessening of the electron hole-recombination process.

Figure S1 depicts the CVs recorded for Ag/CNT₄₀₀, Ag/graphene₄₀₀ and Ag/CNT-graphene₄₀₀ electrodes at a scan rate of 100 mV s⁻¹ in the potential window range from -0.4 to 0.5 V in 6.0 M KOH solution. The CV of CNT-graphene₄₀₀ indicates a cathodic peak at 0.015 V and an anodic one at 0.07 V. Ag incorporation has stimulated shifting both of the peaks into lower potentials elucidating beside its good encapsulation the higher conductivities and ions charge transfer. Conclusively, the CV curves indicate the presence of quasi-capacitance current with an extended potential window in case of the Ag/CNT-G catalyst. This is a good indicative to stability and strong interaction of Ag within CNT-G hybrid than in case of Ag/CNT and Ag/G where

the dissolution of Ag is attained at $100\,\mathrm{mV}$ (Ghilane et al., 2007).

Catalytic Reaction

To confirm thephotocatalytic activity of the catalysts, a nitrophenol (NP) reduction in the presence of 0.5 mmole NaBH4 at room temperature was carried out. The results of all the catalysts; visualized by monitoring the absorption of the reaction mixture at 400 nm (**Figure 8**), showed a full conversion (100%) into p-aminophenol (4-AP) in the activity sequence of; 4%Ag/CNT-graphen400 (210 s) >4%Ag/CNT400 (300 s) >4%Ag/graphene400 (370 s). Accordingly, the calculated kinetics seen as inset in **Figure 8** which shows first order nature indicate values decrease in the order 0.014 s $^{-1}$ >0.0112 s $^{-1}$ >0.010 s $^{-1}$. The time dependent ultraviolet-visible spectra of the reaction mixture in the presence of 4%Ag/CNT-graphen400 showed a gradual decrease in the peak intensity (at 400 nm) of 4-nitrophenolate ions with a gradual increase in the peak intensity (at 300 nm) of 4-AP. The yellow color of the solution



completely fades within 3.5 min reaction time, specifying the over-all conversion of 4-NP to 4-AP. This enhanced activity of the composite CNT-graphene containing Ag is primarily related to increasing the pore volume of this specific catalyst $(0.49~{\rm cm}^3/{\rm g})$ and to the presence of three types of pores in the margin from 1.8 to 4.0 nm in front of only one modal type of pores for the rest of the catalysts. This indeed maximizes the adsorptive capability toward the reactants 4-NP and NaBH₄ and thus helps the facile reduction-capability. It seems also that the particle size decrement was not the main factor affecting the reduction process since $4\%{\rm Ag/CNT_{400}}$ presented the lowest domain $(7~{\rm nm})$ and was not the most reactive catalyst. However, the high

disperse-ability of the Ag nanoparticles with the appreciable surface area the composite own helps much in improving activity, as TEM and N_2 adsorption explores. Exposing the lattice plane (200) on Ag/CNT-graphene₄₀₀ in front of (220) for rest of the catalysts might advocate higher binding energy between 4-NP and the former plane facilitating the reduction process.

The photoreduction performance of 4%Ag/CNT-graphen₄₀₀ toward 4-NP reduction under visible light irradiation ($\lambda > 420$ nm—**Figure 8**), demonstrated an optimal photoreduction performance in 120 s with a rate constant 0.039 s⁻¹ exceeding that in the dark by 2.8 times. There is no reaction occur in the absence of NaBH₄ under irradiation of visible light

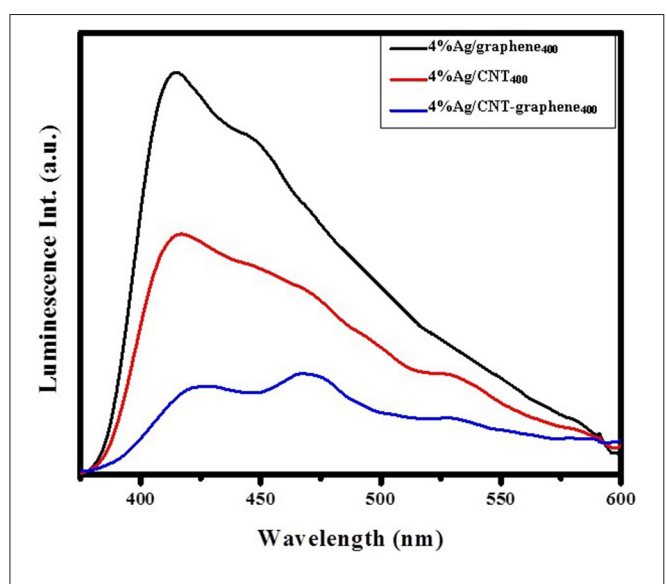


FIGURE 7 | Photoluminescence emission spectra of 4%Ag/graphene₄₀₀, 4%Ag/CNT₄₀₀, and 4%Ag/CNT-graphene₄₀₀ catalysts excited at 320 nm.

confirming the necessity of the catalyst. This extraordinary high activity exceeds many in literatures such as Ag@carbon yolk-shell nanoparticles, ternary Cu₂O–Cu–CuO nanocomposite, Fe₃O₄@SiO₂-Ag, HNTs/Ag, and Ag–NP/C (Tang et al., 2010; Chi et al., 2012; Das and Jana, 2015; Sasmal et al., 2016; Wang et al., 2017). This extensive enhancement in photoreduction performances of 4%Ag/CNT-graphene₄₀₀ proposes more successful separation of electron–hole pairs; as confirmed by PL, and that more photoelectrons were involved in the photo-reduction reaction. The result indicated that the intimate integration of Ag/CNT₄₀₀ with graphene is efficiently initiated the photoreduction performances of 4-NP into 4-AP.

To affirm the latter interface, the flat-band potentials (E_{FB}) for all catalysts in comparison with the Ag free hybrid were determined via the extended linear part of the Mott-Schottky (M-S) plots $\left[\frac{1}{C^2}\right] = \frac{2}{\varepsilon \varepsilon_o e A^2 N_d} \left(V - V_\theta - \frac{k_B T}{e}\right)$ to the x-axis. As shown in **Figure 9**, the positive slopes of the M-S plots seen for all Ag incorporated samples are diagnostic to the n-type semiconductors. On the other hand, CNT-graphene indicated a P-type nature because of the defects and edges could be produced on their surfaces and to the acceptor defects formed due to the vacant oxide species cover their surfaces (Yoo et al., 2014). The E_{FB} of the samples are $-0.018\,V$, $-2.2\,V$, and $-0.05\,V$ for 4%for Ag/CNT-graphene₄₀₀, 4%Ag/CNT₄₀₀, 4% Ag/graphene₄₀₀, respectively in front of 1.4 V (vs. Ag/AgCl) for CNT-graphene₄₀₀. Thus, the values determined for the CB are -0.22, -2.4, -0.25, and 1.2 V for the above sample sequence ($C_B \approx E_{FB} - 0.2 \, V$) (Dong et al., 2017). Apparently, the M-S plot of the CNTgraphene₄₀₀ of a negative slope and a flat band potential of 1.4 V, reflects the increase of the hole carriers density. Concurrently, the 4%Ag/CNT₄₀₀ electrode showed the highest positive V_B potential as compared to the others, testifying clearly the high donor density of that catalyst. On the other hand, decreasing the

E_{FB} shift of the 4% Ag/CNT-graphene₄₀₀ electrode signifies the presence of excess of Ag₂O moieties; as discovered previously by the various physicochemical techniques. Therefore, it was reasonable suggesting the formation of p-n heterojunction at which accumulated electrons are not only responsible for the enhancement of reduction performance; as in 4%Ag/CNT₄₀₀, but also the excess of Ag₂O; as a p-type deficient, eligible for more reactants adsorption. Indeed, rising the p-type charges in 4% Ag/CNT-graphene₄₀₀ along with the n-ones in addition to their separation efficacy provide the highest 4-NP reduction. In conformity, the donor density of 4%Ag/CNT₄₀₀ (4.8×10^{18} cm³) was rather larger than 4%Ag/CNT-graphene₄₀₀ (2.5 × 10^{18} cm³) under dark condition, manifesting that the depletion of electrons in the latter was faster in favor of Ag₂O formation and indeed confirm the p-n interface formation and the role of the latter in achieving high reduction performance.

For investigating the catalytic mechanism and to unravel the effect of some organics on the reduction consequences of 4-NP, several scavengers were utilized to determine the primary active species responsible for the reduction performances of 4%Ag/CNT-graphen₄₀₀. Specifically, triethanol amine (TEOA) isopropanol (IPA), and benzoquinone (BQ) were selected as the main scavengers for the holes, (h+), hydroxyl radicals (\bullet OH), and superoxide radicals (\bullet O₂), respectively. As shown in Figure 10, the catalytic reduction performance of 4%Ag/CNT-graphen₄₀₀ toward 4-NP is changed following the previous additives to imply the following sequence; TEOA < IPA < BQ. On the other hand, the most influential retarder was Na₂CO₃ since it consumes major amounts of Ag₂O and thus decreases accessively the amount of Ag nanoparticles chiefly responsible for the 4-NP reduction. Boosting the activity as a function of light illumination presumes the role played by the holes of Ag₂O (ptype) in capturing some electrons (from CNT due to differences in work function) and thus prolonged the distances between electrons and holes to give enough space for facilely perform the reduction process. Rising the activity on the 4%Ag/CNTgraphen₄₀₀ catalyst might also highlight the necessity of the positively charged Ag₂O p-type in stimulating strong interaction with the -NO₂ group of 4-NP, through the coulombic interaction forces. In addition, the components of Ag₂O can acquire efficient electrons via a transfer process from metallic Ag to efficiently inhibit the recombination of the photo-excited pairs of the latter. Undeniably, few of photo-generated electrons can be captured by the O2 moieties embedded on CNT and graphene surfaces; established via FTIR, to form O₂; assessed from the additive study, to finally affects the activity. The hole transfer on the other hand can react with H₂O or OH[−] to form OH• upon light illumination; as scavengers study confirm, those affect the activity via degradation consequences. Accordingly, the marked decrease in the activity during the addition of IPA and BQ is attributed to the abstraction of H⁺ ions from borohydride to •OH and O₂•moieties and thus influences the reduction consequences.

The mechanism of the catalytic reduction of 4-NP by the Ag@CNT-graphene₄₀₀ catalyst can be proceeded by the diffusion of BH_4^- and 4-NP from the aqueous solution to the Ag nanosurfaces (Huang et al., 2010). Therefore, electron transfer from BH_4^- and CNT/graphene to 4-NP mediated by the $Ag_2O@Ag$

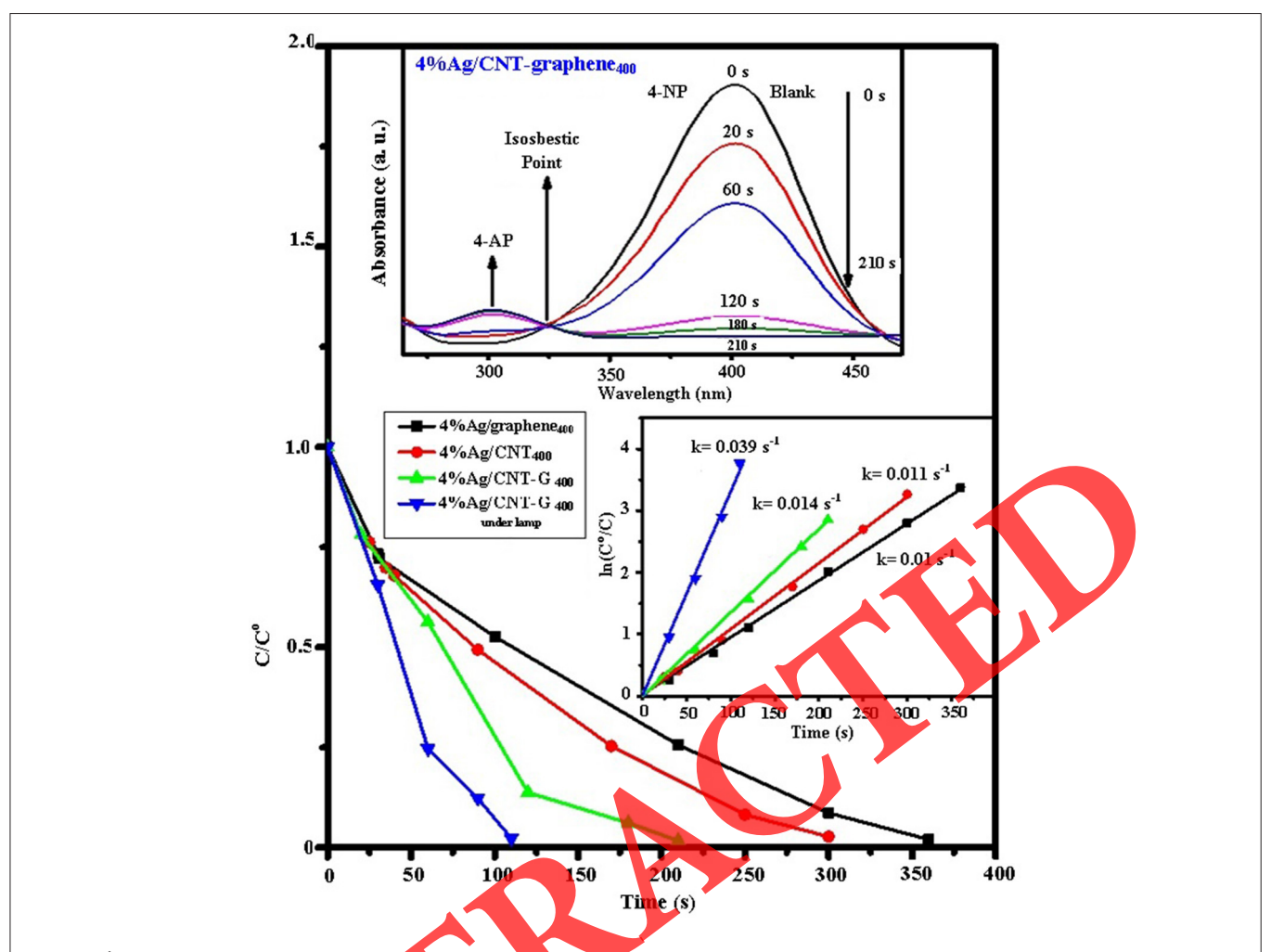
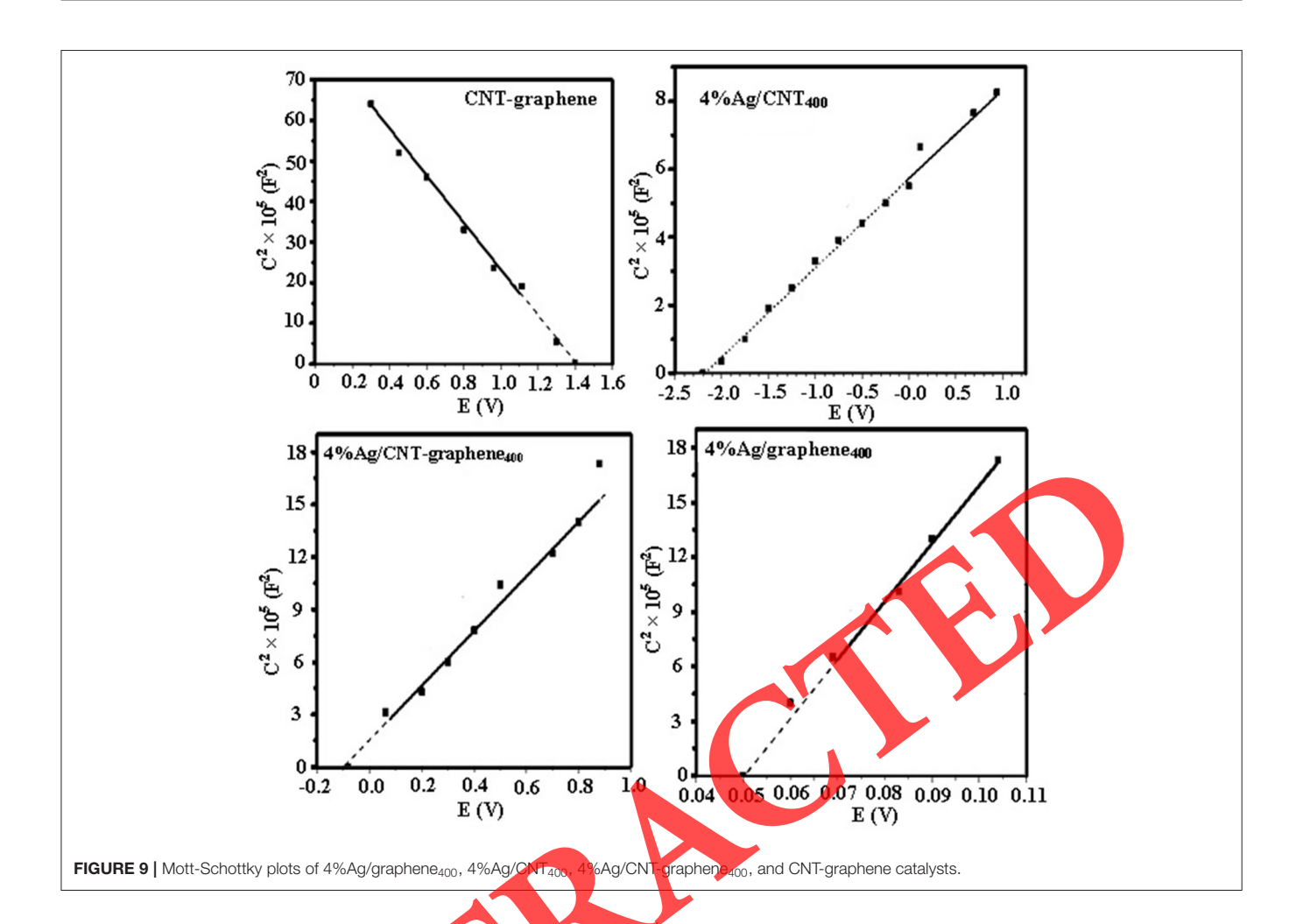


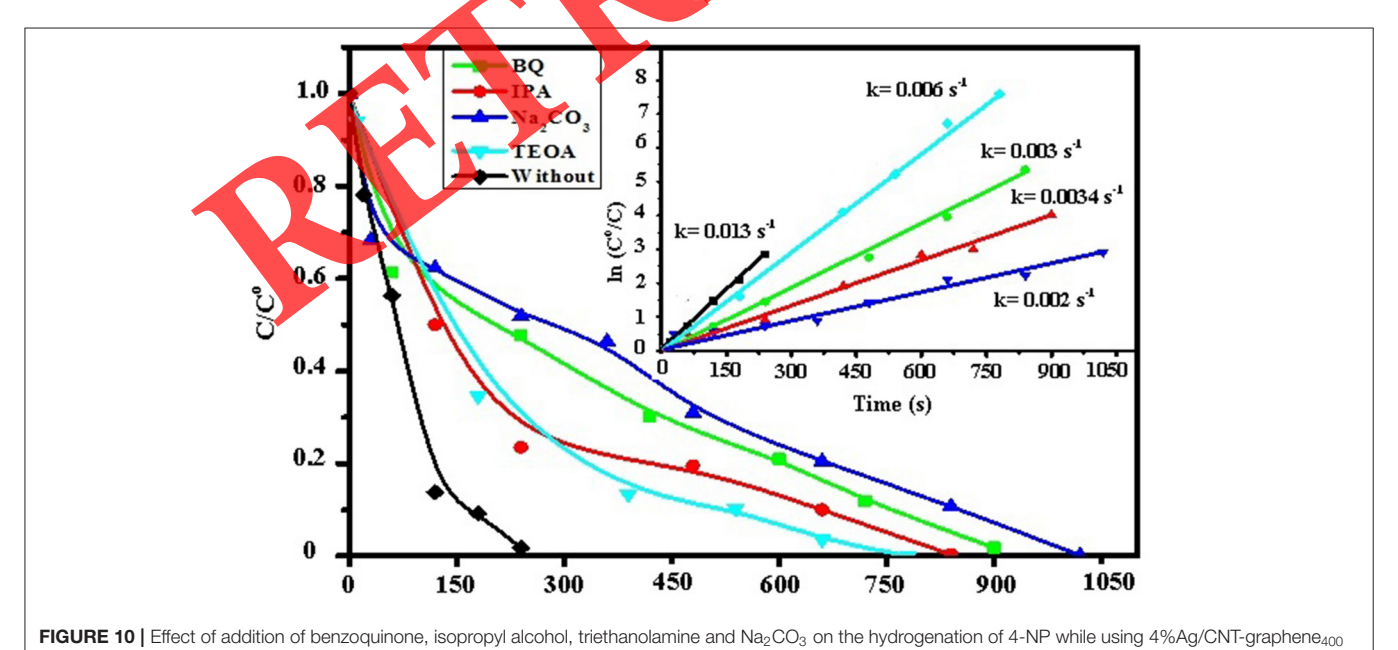
FIGURE 8 | C/C_o vs. time for the hydrogenation of 4-NP over the different catalysts under dark and visible light and pseudo-first-order plots of In (C_o/C) against reaction time for the hydrogenation of 4-NP over the different catalysts (as inset). UV-vis absorption spectra of 4-NP before and after adding NaBH₄ and its reduction product 4-AP with time intervals on 4%Ag/CNT graphere.

interface is expected. Evidently, lowering the work function of Ag (4.26 eV) than that of CNT-graphene (~4.95 eV) rearranges the charges distribution to be around the CNT-graphene composite and thus enhances the reduction efficacy due to the absorption ability of the composite (Huang et al., 2011). The mediated Ag₂O implies high electron density sufficient to promote the reduction reaction with its own as Cu₂O nanoparticles used to show (Zuo et al., 1999). This is chiefly based on decreasing particles size to the nano-range and thus promotes the hybridization of the 3d states with 4sp-states, decreasing the former population and to enhance the reactant adsorption, to boost the catalytic reaction (Hammer and Nørskov, 1995). Such hybridization process also shifts the occupied states of the surface to higher energies, which favors bond formation with the reactants.

Figure 11 presents the galvanostatic charge/discharge (CD) curves of 4%Ag/CNT₄₀₀, 4%Ag/CNT-graphene₄₀₀, and 4%Ag/graphene₄₀₀ electrodes at a current density of 1 A g⁻¹ within a potential range extends from -0.54 to -0.14 V. As shown in the **Figure 11**, all the curves display a symmetrical

triangle shape with slight distortion, indicating high reversibility of the composites during charge/discharge processes. As expected, the 4%Ag/CNT-graphene₄₀₀ composite electrode shows the longer charge-discharge time exceeding in sequence 4%Ag/CNT₄₀₀ and 4%Ag/graphene₄₀₀. The specific capacitance in sequence calculated from the CD curves via using the equation: C = It/mV, at 1 A g^{-1} , are 355, 230.0, and 185.8, F g^{-1} , respectively. Consistent with the CV results, the specific capacitance of the 4%Ag/CNT-graphene₄₀₀ electrode was much higher than rest of the electrodes, demonstrating the excellent synergistic effect of the 4%Ag/CNT-graphene₄₀₀ electrode. The specific capacitance of the latter electrode is found to increase with the contents of Ag₂O in the composite and it's about 1.5 times higher than that of the 4%Ag/CNT₄₀₀ electrode at the same current density. This enhancement may explain the contribution of the high concertation of the conductive Ag₂O@Ag in facilitating charge transport and energy storage within the CNT-graphene network. Evidently, the specific capacitance of the 4%Ag/CNT-graphene₄₀₀ electrode is much larger than the





together with In Co/C against time curves as inset.

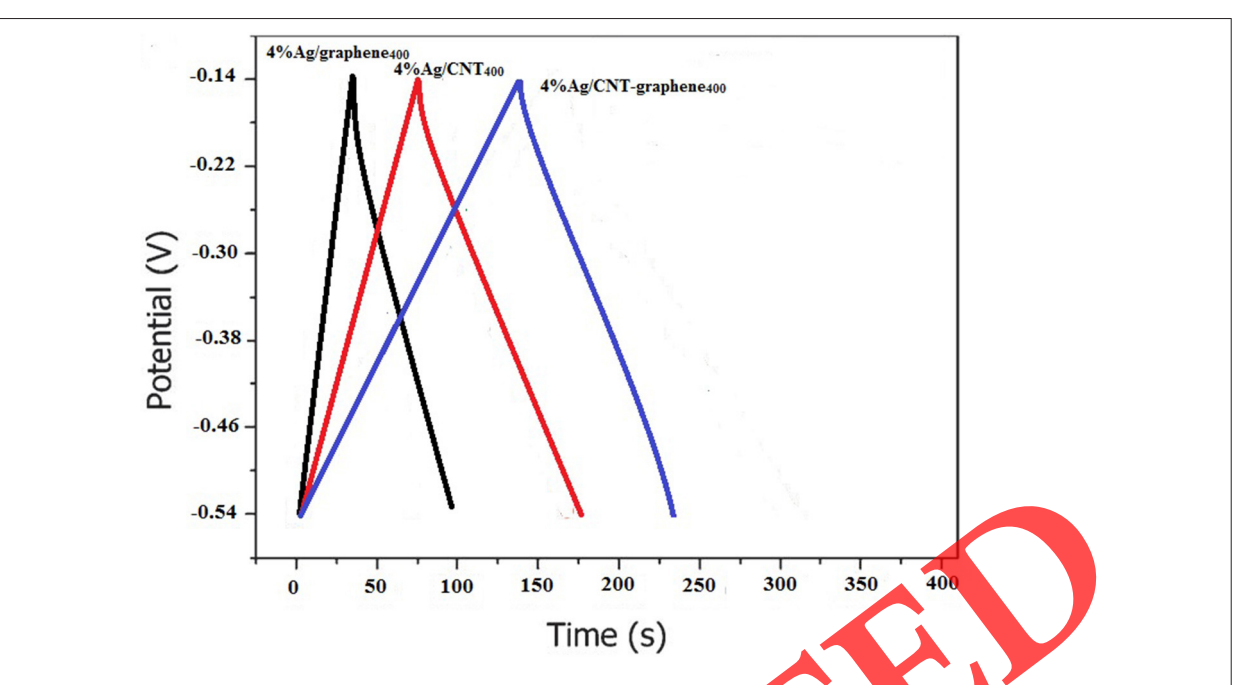


FIGURE 11 | The galvanostatic charge-discharge curves of 4%Ag/graphene₄₀₀, 4%Ag/CNT₄₀₀ and 4%Ag/CNT-graphene₄₀₀ electrodes during current density of 1.0 A g⁻¹ in 6.0 M KOH electrolytes.

reported value of the tubular Ag/MnOx nanosheets (170 F g⁻¹ at 1 mV s⁻¹) (Zhang et al., 2015). It also surpasses the specific capacitance value of the Ag/MnO2 nanocomposite (185.5 F g⁻¹ at 0.5 A g⁻¹) (Li et al., 2014) and those of Ag/PANI (75 F g⁻¹) (Lu et al., 2016), Ag-GNFs/PANI (212 F g⁻¹ at 0.1 A g⁻¹) (Min et al., 2014), (PPY)/PAA)/Ag composite electrode (226 F g⁻¹ at 10 mV s⁻¹), and Ag/manganese dioxide films (225 F g⁻¹ at 2 mVs⁻¹) (Seok et al., 2012; Patil et al., 2013), it also exceeds the assynthesized Mn₃O₄-graphene that exhibits specific capacitance of 236.7 F. g⁻¹ at 1 A g⁻¹ as well as the blended graphene-SWCNT composite film that indicates specific capacitance of 290.6 F g⁻¹ at 1 A g⁻¹ (Cheng et al., 2013); Wang et al., 2012).

Combining the CD and surface texturing analysis reveals that the surface areas are not persistently lead the specific capacitance values but rather the deep pore volume and pore structure are rather dominating. This result also highlights that the composite CNT-graphene was the one responsible for increasing in the specific capacitance for many reasons most importantly is the high conductivity of CNT facilitating the transportation of electrons and ions and also the tangled CNT can react efficiently with graphene preventing its agglomeration to exhibit lower resistance.

To examine and to understand the charge transfer efficiency of generated charge carriers in the interfacial region, EIS measurements were performed. Generally, a smaller semicircle arc radius specifies a faster interfacial charge transfer rate over a semiconductor material. As shown in **Figure 12**, arc radii of different catalysts follow the order of: 4%Ag/CNT-graphene₄₀₀ <4%Ag/CNT-graphene₄₀₀ . This indicates that 4%Ag/CNT-graphene₄₀₀ possesses the smallest charge transfer resistance in the interfacial zone, and implies the beneficial of

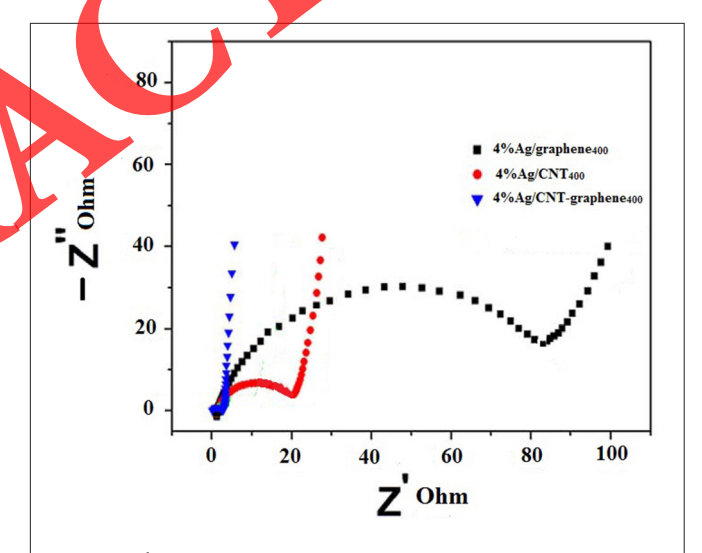
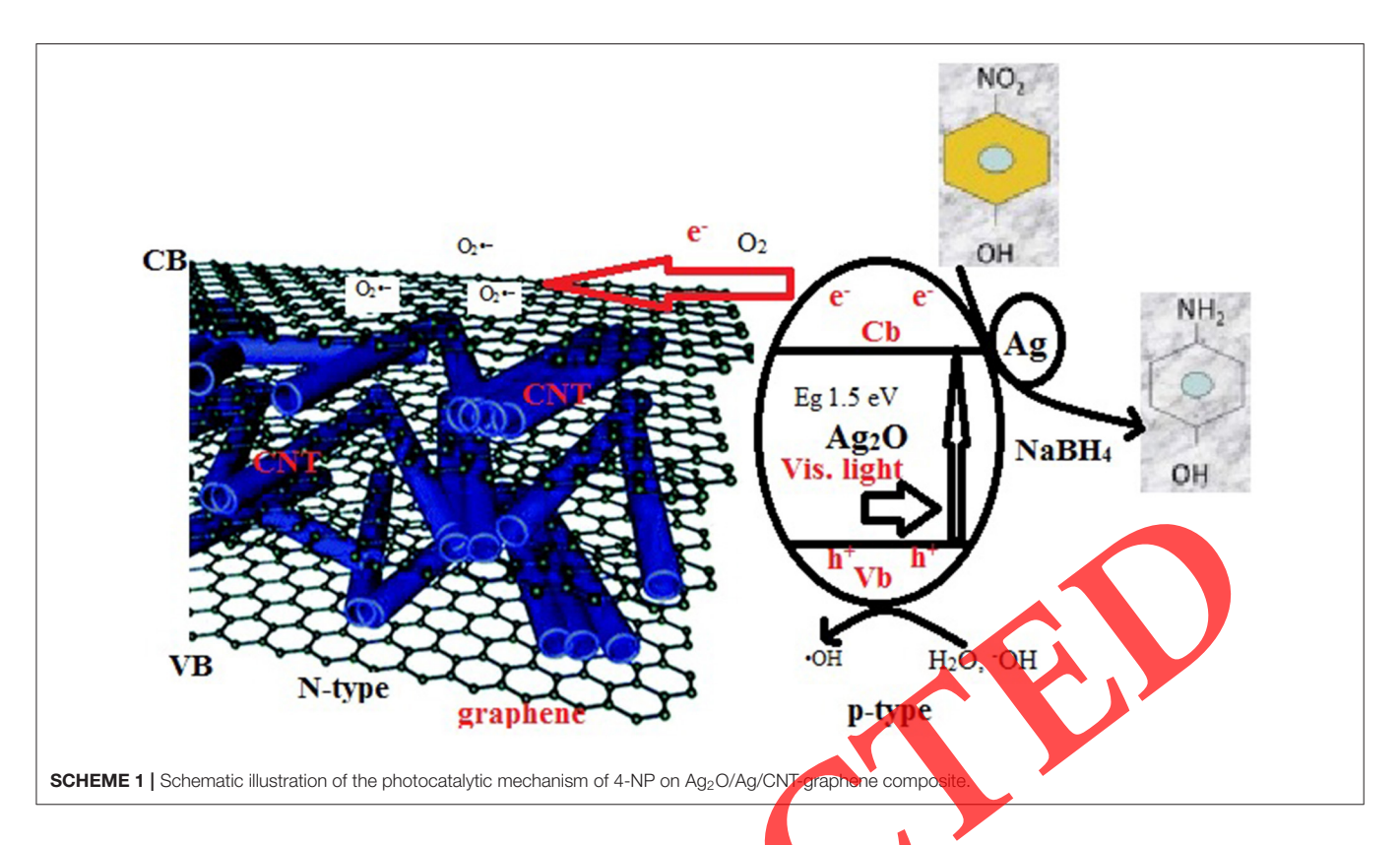
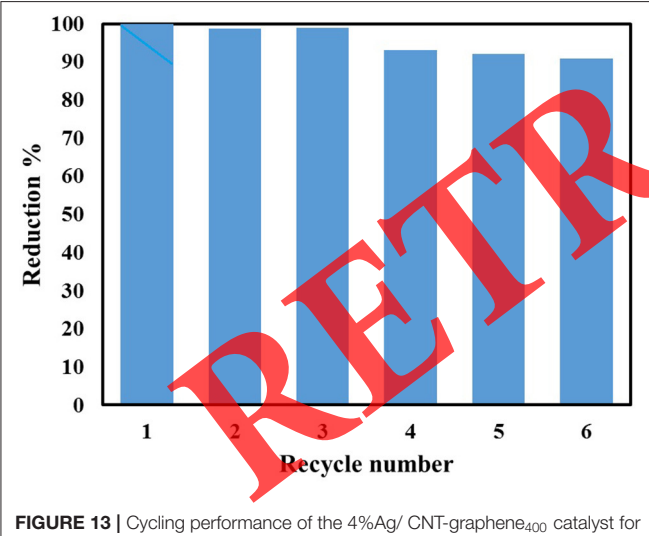


FIGURE 12 | Electrochemical impedance spectra (EIS) of 4%Ag/graphene₄₀₀, 4%Ag/CNT₄₀₀ and 4%Ag/CNT-graphene₄₀₀ electrodes at room temperature in 6.0 M KOH.

CNT-graphene in boosting the charge transfer efficiency of the Ag_2O/Ag species. This demonstrates that R_{ct} is considerably reduced by introducing graphene into Ag/CNT to form dual p-n junctions via Ag_2O/CNT -graphene [p-type] with metallic Ag [n-type], which can substantially promote the separation efficiency and suppress the recombination ratio of charge carriers.

It should be emphasized that EIS results are consistent with the (photo)-activities of the different catalysts, PL results and to the synergistic interaction between Ag₂O and Ag





4-NP reduction.

moieties on CNT-graphene, established via CV, FTIR, and Raman results. EIS results also indicated the smallest intercept for 4%Ag/CNT-graphene₄₀₀, which integrated the electrolyte solution resistance and contact resistance at the interface of the active material/current collector. Increasing the slope of the latter comparatively provides the sample best capacitance based on the excellent ions diffusion into the interior of the composite besides the aforementioned good charge transfer and low internal resistance.

d on the above methodical exploration, a conceivable photocatalytic mechanism of the Ag₂O/Ag/CNT-graphene rnary heterostructure is proposed, as strongly illustrated in Scheme 1. Under Visible light irradiation, the bandgap photoexcitation of Ag₂O components (p-type) occurs, by exciting electrons (e⁻) from the V_B to the corresponding C_B, leaving holes (h⁺) in the V_B. Immediately, the electrons are instantly captured by CNT-graphene to rapidly transferred to the O₂ dissolved in the reaction medium or those on the composite surfaces; established via FTIR, to produce superoxide radicals $(O_2 \bullet -)$ that contribute in delaying the reduction consequences but most importantly postponing the charges recombination process. Thus, some of the electrons are involved in the reduction of 4-NP to 4-AP that indeed remarkably assisted by the metallic Ag moieties. The holes on the other hand can react with $H_2O/^-OH$ species to form hydroxyl radicals ($\bullet OH$); emphasized from the scavenger study. Such processes occurred over Ag₂O can retard the e--h+ recombination and indeed prolong their life time to result in an enhanced catalytic performance of the Ag₂O/Ag/CNT-graphene heterostructure. Furthermore, the intimate interfacial contact among the hybrid in assembling P-n units in conjunction with their cooperative synergy also contributes to the enhanced (photo)catalytic performance of the ternary hetero-structure.

The durability of the 4%Ag₂O/Ag/CNT-graphene₄₀₀ catalyst toward 4-NP reduction was tested via performing 6 successive runs under visible light illumination and without any treatment between the runs. Figure 13 explores the excellent recyclability and reusability via achieving activity comprised of 92%. This successful recycling informs that the structure of the catalyst is still intact and do not change under the excessive reaction conditions of $NaBH_4$ and under illumination. It also dictates the stabilization of both the metal oxide and the NPs via considerable interaction with composite of CNT and graphene preventing them from leaching during the reaction.

CONCLUSIONS

The established heterostructure Ag₂O@Ag@CNT-graphene has shown fascinating photo-reduction performances for 4-NP with a rate constant of 0.039 s⁻¹ exceeding many in literatures and indicates a magnificent specific capacitance value of 355 F g⁻¹ at 1.0 A g⁻¹. Although this photocatalyst does not reflect the highest number of charge carriers it exposes appreciable amounts of Ag₂O (p-type) that played a unique role toward the reactants adsorption and to contribute with the metallic Ag in enhancing the mentioned applications. This study also highlights the synergistic effects prompted by the constructed 3D-like array via 1D CNT (as spacer) and 2D graphene in dispersing Ag₂O and Ag nanoparticles. The electronic conductivity of latter moieties, the porous nature of the composite, the p-n junction

REFERENCES

- Armani, M. A., Abu-Taleb, A., Remalli, N., Abdullah, M., Srikanth, V. V. S. S., and Labhasetwar, N. K. (2016). Dragon's blood-aided synthesis of Ag/Ag₂O core/shell nanostructures and Ag/Ag₂O decked multi-layered graphene for efficient As(III) uptake from water and antibacterial activity. RSC Adv. 6, 44145–44152. doi: 10.1039/C6RA05061A
- Broza, G., Kwiatkowska, M., Rosłaniec, Z., and Schulte, K. (2005). Processing and assessment of poly(butylene terephthalate) nanocomposites reinforced with oxidized single wall carbon nanotubes. *Polymer* 46, 5860–5867. doi:10.1016/j.polymer.2005.05.073
- Carboni, D., Marongiu, D., Rassu, P., Pinna, A., Amenitsch, H., Casula, M., et al. (2014). Enhanced photocatalytic activity in low-temperature processed titania mesoporous films. J. Phys. Chem. C 118, 12000–12009. doi: 10.1021/jp501653x
- Cheng, Q., Tang, J., Ma, J., Zhang, H., Shinya, N., and Qin, L. C. (2011). Graphene and carbon nanotube composite electrodes for supercapacitors with ultra-high energy density. *Phys. Chem. Chem. Phys.* 13, 17615–17624. doi:10.1039/c1cp21910.
- Chi, Y., Yuan, Q., Li, Y., Tu, J., Zhao, L., El, N., et al. (2012). Synthesis of Fe₃O₄@SiO₂-Ag magnetic nanocomposite based on small-sized and highly dispersed silver nanoparticles for catalytic reduction of 4-nitrophenol. *J. Colloid Interface Sci.* 383, 96–102. doi: 10.1016/j.jcis.2012.06.027
- Das, S., and Jana, S. (2015). A facile approach to fabricate halloysite/metal nanocomposites with preformed and in situ synthesized metal nanoparticles: a comparative study of their enhanced catalytic activity. *Dalton Trans.* 44, 8906–8916. doi: 10.1039/C5DT00830A
- Dong, M. W., Liu, C., and Luo, S. (2017). Silver phosphate-based Z-Scheme photocatalytic system with superior sunlight photocatalytic activities and anti-photocorrosion performance. *Appl. Catal. B* 208, 1–13. doi:10.1016/j.apcatb.2017.02.065
- Eda, G., and Chhowalla, M. (2010). A facile strategy for the preparation of mos3 and its application as a negative electrode for supercapacitors. *Adv. Mater. Weinheim.* 22, 2392–2398. doi: 10.1002/adma.2009 03689
- Geim, A. K. (2009). Tuning the redox properties of cobalt particles supported on oxides by an in-between graphene layer. Science 324, 1530–1536. doi: 10.1126/science.1158877

interface and delaying of e⁻-h⁺ recombination together with decreasing the internal resistance are all competes in enhancing the photoreduction and energy storage reactions.

AUTHOR CONTRIBUTIONS

MM suggest synthesize of $Ag_2O@Ag@CNT$ -graphene catalyst with varied amounts of $Ag_2O@Ag$ and compared with the individual analog of Ag/CNT and Ag/graphene. He participate in discussion and writing of this search. MK participate in discussion, writing of this search and preparation of substances under study. AI participate in synthesize of materials and analysis of materials by XRD, TEM, Raman, FTIR, UV-Vis Diffuse reflectance, N_2 adsorption beside electrochemical techniques such as cyclic voltammetry (CV), galvanostatic charge-discharge, and impedance spectroscopy (EIS).

SUPPLEMENTARY MATERIAL

The Supplementary Material for this article can be found online at: https://www.frontiersin.org/articles/10.3389/fchem. 2018.00250/full#supplementary-material

- Geim, A. K., and Novoselov, K. S. (2007). The rise of graphene. *Nat. Mater.* 6, 183–189. doi: 10.1038/nma.1849
- Ghilane, J., Fan, F. F., and Bard, A. J. (2007). Facile electrochemical characterization of core/shell nanoparticles. Ag Core/Ag₂O shell structures. *Nano Lett.* 7, 1406–1412. doi: 10.1021/nl070268p
- Guo, Z., Chen, Y. T., Li, L. S., Wang, X. M., Haller, G. L., and Yang, Y. H. (2010). Carbon nanotube-supported Pt-based bimetallic catalysts prepared by a microwave-assisted polyol reduction method and their catalytic applications in the selective hydrogenation. *J. Catal.* 276, 314–326. doi: 10.1016/j.jcat.2010.09.021
- Hammer, B., and Nørskov, J. K. (1995). Nanoparticle-cell interactions: relevance for public health. *Nature* 376, 238–245. doi: 10.1038/376238a0
- Han, Z. Z., Ren, L. L., Cui, Z. H., Chen, C. Q., Pan, H. B., and Chen, J. Z. (2012). Ag/ZnO flower heterostructures as a visible-light driven photocatalyst via surface plasmon resonance. Appl. Catal. B 126, 298–305. doi: 10.1016/j.apcatb.2012.07.002
- Hu, C. G., Wang, W. L., Liao, K. J., Liu, G. B., and Wang, Y. T. (2004). Systematic investigation on the properties of carbon nanotube electrodes with different chemical treatments. J. Phys. Chem. Solids 65, 1731–1736. doi: 10.1016/j.jpcs.2004.04.009
- Huang, J. H., Fang, J. H., Liu, C. C., and Chu, C. W. (2011). Electrochemical properties of carbon nanotube/graphene oxide hybrid electrodes fabricated via layer-by-layer self-assembly. ACS Nano. 23, 6262–6271. doi: 10.1021/nn201253w
- Huang, J., Zhang, L., Chen, B., Ji, N., Chen, F., Zhang, Y., et al. (2010). Nanocomposites of size-controlled gold nanoparticles and graphene oxide: formation and applications in SERS and catalysis. *Nanoscale* 2, 2733–2738. doi:10.1039/c0nr00473a
- Ibrahim, I., Ali, I. O., Salama, T. M., Bahgat, A. A., and Mohamed, M. M. (2016). Synthesis of magnetically recyclable spinel ferrite (MFe $_2$ O $_4$, M = Zn, Co, Mn) nanocrystals engineered by sol gel-hydrothermal technology: high catalytic performances for nitroarenes reduction. *Appl. Catal. B* 181, 389–402. doi: 10.1016/j.apcatb.2015.08.005
- Li, Y. H., Fu, H. Y., Zhang, Y. F., Wang, Z. Y., and Li, X. D. (2014). Kirkendall effect induced one-step fabrication of tubular Ag/MnO_X nanocomposites for supercapacitor application. *J. Phys. Chem. C* 118, 6604–6611. doi: 10.1021/jp412187n

- Liu, X., Li, H., Zeng, Q., Zhang, Y., Kang, H., Duan, H., et al. (2015). Electro-active shape memory composites enhanced by flexible carbon nanotube/graphene aerogels. *Mater. Chem. A* 3, 11641–11649. doi: 10.1039/C5TA02490K
- Lu, S., Yan, D., Chen, L., Zhu, G., Xu, H., and Yu, A. (2016). One-pot fabrication of hierarchical Ag/MnO₂ nanoflowers for electrochemical capacitor electrodes. *Mater. Lett.* 168, 40–43. doi: 10.1016/j.matlet.2016.01.021
- Min, J., Haeri, K., Akbar, J., Inamdar, I., Jo, Y., Han, J. K. et al. (2014). Synthesis and enhanced electrochemical supercapacitor properties of Ag-MnO₂-polyaniline nanocomposite electrodes. *Energy* 70, 473–477. doi:10.1016/j.energy.2014.04.018
- Mohamed, M. M., Khairy, M., and Eid, S. (2017). Surfactant-assited formation of silver titanates as active catalysts for methanol electro-oxidation. *Appl. Catal. A* 547, 205–213. doi: 10.1016/j.apcata.2017.08.031
- Patil, D. S., Pawar, S. A., Devan, R. S., Gang, M. G., Ma, Y. R., and Hyeok, J. (2013). Electrochemical supercapacitor electrode material based on polyacrylic acid/polypyrrole/silver composite. *Electrochim. Acta* 105, 569–577. doi: 10.1016/j.electacta.2013.05.022
- Sasmal, A. K., Dutta, S., and Pal, T. (2016). A ternary Cu₂O-Cu-CuO nanocomposite: a catalyst with intriguing activity. *Dalton Trans*. 45, 3139–3150. doi: 10.1039/C5DT03859F
- Seok, K., Soo, K., and Park, J. (2012). Bridge effect of silver nanoparticles on electrochemical performance of graphite nanofiber/polyaniline for supercapacitor. Synth. Metals 162, 2107–2111. doi:10.1016/j.synthmet.2012.09.021
- Sheng, Z. H., Gao, H. L., Bao, W. J., Wang, F. B., and Xia, X. H. (2012). Synthesis of boron doped graphene for oxygen reduction reaction in fuel cells. *J. Mater. Chem.* 22, 390–395. doi: 10.1039/C1JM14694G
- Sun, D. M., Liu, C., Ren, W. C., and Cheng, H. M. (2013). A review of carbon nanotube- and graphene-based flexible thin-film transistors. Small 9, 1188–1205. doi: 10.1002/smll.201203154
- Tang, S., Vongehr, S., and Meng, X. (2010). Carbon spheres with controllable silver nanoparticle doping. J. Phys. Chem. C 114, 977–982. doi: 10.1021/jp91 02492

- Wang, D., Li, Y., Wang, Q., and Wang, T. (2012). Facile synthesis of porous Mn₃O₄ nano-crystal-graphene nanocomposites for electrochemical supercapacitors. Eur. J. Inorg. Chem. 2012, 628–635. doi: 10.1002/ejic.201100983
- Wang, D., Zhao, B., Jiang, Y., Hu, P., Gao, D., and Zhang, H. (2017). Self-etching preparation of yolk-shell Ag@carbon nanostructures for highly effective reduction of 4-nitrophenol. *Catal. Commun.* 102, 114–117. doi: 10.1016/j.catcom.2017.09.007
- Wang, Y., Shi, Z., and Yin, J. (2010). Unzipped multiwalled carbon nanotubes for mechanical reinforcement of polymer composites. J. Phys. Chem. C 114, 19621–19628. doi: 10.1021/jp107151e
- Yoo, S., Li, X., Wu, Y., Liu, W., Wang, X., and Yi, W. (2014). Recent progress on graphene-based hybrid electrocatalysts. J. Nanomater. 214, 1–6. doi:10.1155/2014/497384
- Zhang, L., Wang, W. Z., Jiang, D., Gao, E. P., and Sun, S. M. (2015). Photoreduction of CO₂ on BiOCl nanoplates with the assistance of photoinduced oxygen vacancies. *Nano. Res.* 8, 821–831. doi: 10.1007/s12274-014-0564-2
- Zhao, Y., Xie, Y., Yu, Y., Tang, H. L., Jie, W., Jiang, Y., et al. (2013). Bioactive calcium phosphate compounds. *J. Mater. Chem. C* 1, 4956–4963. doi: 10.1039/c3tc30743c
- Zuo, J. M., Kim, M., O'Keeffe, M., and Spence, J. C. H. (1999). Experimental observation of charge-shift bond in fluorite Cat., *Nature* 401, 49–55.

Conflict of Interest Statement: The authors declare that the research was conducted in the absence of any commercial or financial relationships that could be construed as a potential conflict of interest.

Copyright © 2018 Mohaned, Khair) and Ibrahem. This is an open-access article distributed under the terms of the Creative Commons Attribution License (CC BY). The use, distribution or reproduction in other forums is permitted, provided the original author(s) and the copyright owner(s) are credited and that the original publication in this journal is cited, in accordance with accepted academic practice. No use, distribution or reproduction is permitted which does not comply with these terms.